Spin and orbital transport in rare-earth dichalcogenides: The case of EuS_2

Mahmoud Zeer,[1,2,*] Dongwook Go,[1,3,†] Johanna P. Carbone,[1,2] Tom G. Saunderson,[3] Matthias Redies,[1,2] Mathias Kläui,[3] Jamal Ghabboun,[4] Wulf Wulfhekel,[5] Stefan Blügel,[1] and Yuriy Mokrousov[1,3,‡]

[1]*Peter Grünberg Institute and Institute for Advanced Simulation, Forschungszentrum Jülich and JARA, 52425 Jülich, Germany*

[2]*Department of Physics, RWTH Aachen University, 52056 Aachen, Germany*

[3]*Institute of Physics, Johannes Gutenberg-University Mainz, 55099 Mainz, Germany*

[4]*Department of Physics, Bethlehem University, Bethlehem, Palestine*

[5]*Physikalisches Institut, Karlsruhe Institute of Technology, 76131 Karlsruhe, Germany*

(Received 1 February 2022; revised 10 June 2022; accepted 17 June 2022; published 7 July 2022)

We perform first-principles calculations to determine the electronic, magnetic, and transport properties of rare-earth dichalcogenides, taking a monolayer of H-phase EuS_2 as a representative. We predict that the H phase of the EuS_2 monolayer exhibits a half-metallic behavior upon doping with a very high magnetic moment. We find that the electronic structure of EuS_2 is very sensitive to the value of Coulomb repulsion U, which effectively controls the degree of hybridization between Eu f and S p states. We further predict that the nontrivial electronic structure of EuS_2 directly results in a pronounced anomalous Hall effect with nontrivial band topology. Moreover, while we find that the spin Hall effect closely follows the anomalous Hall effect in the system, the orbital complexity of the system results in a very large orbital Hall effect, whose properties depend very sensitively on the strength of correlations. Our findings thus promote rare-earth-based dichalcogenides as a promising platform for topological spintronics and orbitronics.

DOI: 10.1103/PhysRevMaterials.6.074004

I. INTRODUCTION

Two-dimensional (2D) transition-metal dichalcogenides (TMDs) have attracted enormous attention due to their strong potential as a platform for various flavors of spintronics effects. The rich set of electronic phases that TMDs exhibit includes semiconductors [1–3], semimetals [4], metals [5], and superconductors [6], which allows for novel design paradigms incorporating multiple complex phases of matter. Furthermore, due to a combination of low crystal symmetry and spin-orbit coupling (SOC) [7], these materials can host exotic excitations and exhibit different transport properties. For example, recent studies suggested that TMDs naturally lacking inversion symmetry can be exploited to exhibit a variety of Hall effects such as the anomalous Hall effect (AHE) [8], valley Hall effect [9,10], spin Hall effect (SHE) [11,12], or even the orbital Hall effect (OHE) [13–23].

Among the latter two phenomena, the SHE and OHE have attracted particular attention owing to bright prospects for spintronic applications [24–27]. While the SHE is a well-known phenomenon that has, by now, been studied in depth [28], the OHE is much less explored [18,20–22,25]. The essence of the OHE is in the coupling between the orbital motion of electrons and an electric field, which drives a transverse flow of orbital angular momentum, as opposed to spin angular momentum in the SHE [13,15,18,29–31]. Such orbital Hall currents can, for example, generate a measurable effect via the generation of the orbital type of torques on magnetization [32,33] or can give rise to strong nonlocal spin currents via the effect of spin-orbit coupling [34]. This also gives rise to a new channel for information transfer: the orbital channel. Harnessing the physics of orbital currents is expected to push spintronics into a new direction, the direction of orbitronics [35].

On the side of materials, the OHE has been studied predominantly in nonmagnetic systems, and very little is known about orbital currents in magnetic systems, especially in low dimensions. In this light, magnetism in 2D materials can be extremely profitable for spintronics and orbitronics [36–38]. Recent discoveries of magnetic order in various classes of 2D magnets such as CrI_3 [39], Fe_3GeTe_2 [40], and bilayer $Cr_2Ge_2Te_6$ [41,42] have given the exploration of novel 2D ferromagnetic materials and their magnetic properties significant momentum. On the side of TMDs, several representative compounds, such as metallic VX_2 [43–45], CrX_2 [45–47], and semiconducting MnS_2 (X = S, Se, Te) [45,48,49], have been shown to exhibit magnetic ordering in their ground state. A very promising direction to pursue here is the realization of 2D magnetic materials, in particular dichalcogenides, based on $4f$ elements. Given a strong tendency to magnetism and strong SOC combined with the orbital complexity of $4f$ electrons, $4f$-based 2D materials are expected to serve as a fruitful foundation for various spin and, especially, orbital transport effects.

In this work, we perform first-principles calculations of structural, electronic, magnetic, and transport properties of the H-phase monolayer of the $4f$ rare-earth dichalcogenide EuS_2. Taking EuS_2 as an example, we thus aim to uncover the potential of the $4f$ rare-earth dichalcogenides as possible

*m.zeer@fz-juelich.de
†d.go@fz-juelich.de
‡y.mokrousov@fz-juelich.de

sources of pronounced charge, spin, and orbital currents. Keeping in mind the importance of correlation effects in f electron materials, we consider a range of Coulomb strengths as given by the parameter U, finding that EuS_2 has a very large magnetic moment and a large band gap for a wide range of correlation strengths. Importantly, we find a strongly increased p-d-f hybridization among Eu and S atoms upon increasing U, which has a drastic influence on the transport properties. Specifically, our calculations predict that in the strongly correlated limit the electronic bands in EuS_2 have a nontrivial topology, which results in sizable nearly quantized values of the anomalous Hall conductivity (AHC) exhibited by the f states. Remarkably, we find that the SHE in the system largely follows the behavior of the AHE owing to the strong majority character of the occupied f states, while the OHE exhibits a very nontrivial behavior as a function of band filling, reaching a magnitude more than six times larger than that of the SHE. The detailed analysis we have carried out of the electronic structure in conjunction with Hall effects in the EuS_2 makes it possible to grasp the basic principles that can be used to turn rare-earth dichalcogenides into an efficient source of orbital currents. Given the strong tendency of this class of materials to magnetism, we thus propose that rare-earth dichalcogenides can occupy a unique place in the exotic niche of 2D magnetic materials with high potential for spintronics and orbitronics. Our paper is structured as follows: In Sec. II we provide the computational details of our study. In Sec. III we present the results of our calculations and analysis, including a discussion, and we end with a brief discussion in Sec. IV.

II. COMPUTATIONAL DETAILS

Our first-principles calculations were performed using the film version of the full-potential linearized augmented plane wave method [50], as implemented in the Jülich density functional theory (DFT) code FLEUR [51]. We used the Perdew-Burke-Ernzerhof approximation to the exchange-correlation potential [52]. The structure of the monolayer was relaxed so that residual forces are well below 0.001 eV/Å. For self-consistent calculations we used a 16×16 Monkhorst-Pack grid in the first Brillouin zone and a plane-wave cutoff of $4.1a_0^{-1}$, where a_0 is the Bohr radius. We set an angular momentum expansion of 10 and 8 for Eu and S atoms, respectively. The muffin-tin radii of Eu and S atoms were set to $2.8a_0$ and $1.94a_0$, respectively. SOC was included self-consistently within the second variation scheme for all calculations.

To treat the effect of strongly correlated electrons in the $4f$ shell of Eu we applied the GGA+U method within the self-consistent DFT cycle [53]. The on-site Coulomb interaction strength U applied to the Eu $4f$ states was varied from 0 to 6.7 eV, and the intra-atomic exchange interaction strength J was chosen to be 0.7 eV [53]. The optimized structure of H-EuS_2 is shown in Fig. 1 together with the definition of the axes. We first performed structural relaxations without U, which yielded a lattice constant of H-EuS_2 of 4.616 Å and a distance between the planes of the Eu and S atoms along the z axis of 1.1 Å. Adding a Coulomb repulsion strength of $U = 6.7$ eV modified the values of the respective distances

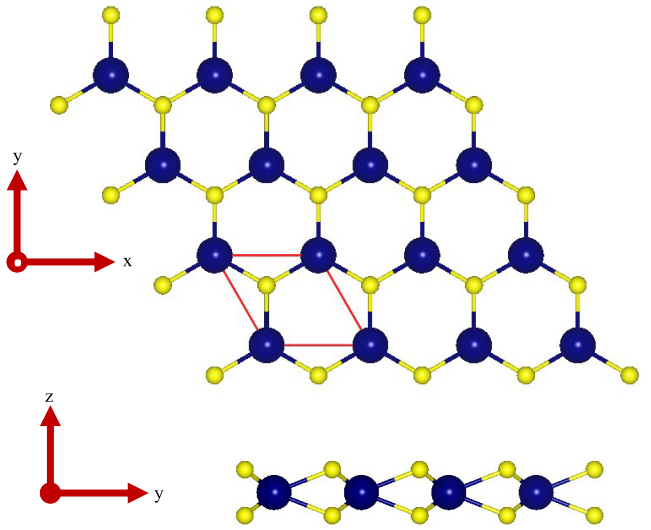

FIG. 1. Top and side views of H-phase monolayer EuS_2. The dark blue balls and yellow balls represent Eu and S atoms, respectively. The definition of the axes is shown with arrows.

to 4.744 and 1.08 Å. All calculations were performed for the latter values of the structural constants.

Transport calculations were performed for two values of U: 2.5 and 6.7 eV. The calculations of the AHC, spin Hall conductivity (SHC), and orbital Hall conductivity (OHC) were performed according to expressions discussed below by exploiting the technique of Wannier interpolation [54,55]. In order to do this, 36 maximally localized Wannier functions (MLWF) were constructed out of the *ab initio* electronic structure by projecting the Bloch states onto p states of S and f and d states of Eu atoms to reproduce the electronic structure in an energy window that contains all the states below the Fermi energy and enough states above the Fermi energy. Throughout this work we treat the system as a perpendicularly magnetized ferromagnet. For $U = 6.7$ eV the magnetic anisotropy energy was estimated to be of the order of 30 μeV, favoring the out-of-plane direction of magnetization, while the ferromagnetic state was found to be 0.3 meV lower in energy than the row-wise antiferromagnetic state. We have to remark that these values may change following changes in the Fermi energy in the system upon doping, which presents the main case of interest in this study (see discussion below).

III. RESULTS AND DISCUSSION

A. Electronic structure of EuS_2

We first discuss the electronic structure of EuS_2. We recall that consistent with Hund's first rule, the intra-atomic exchange interaction arranges the electronic configuration of the half-filled Eu $4f$ shell in the $4f^7$ configuration, giving rise to a large magnetic moment of $6.95\mu_B$, a value which is robust with respect to the correlation strength. This is significantly larger than the spin moments in other TMD materials, compared, e.g., to Refs. [44,48,49]. In Fig. 2 we show the computed band structure of the system [Figs. 2(a)–2(d)], together with the densities of states (DOSs) [Figs. 2(e)–2(h)], for U values of 0 eV [Figs. 2(a) and 2(e)], 2.5 eV [Figs. 2(b)

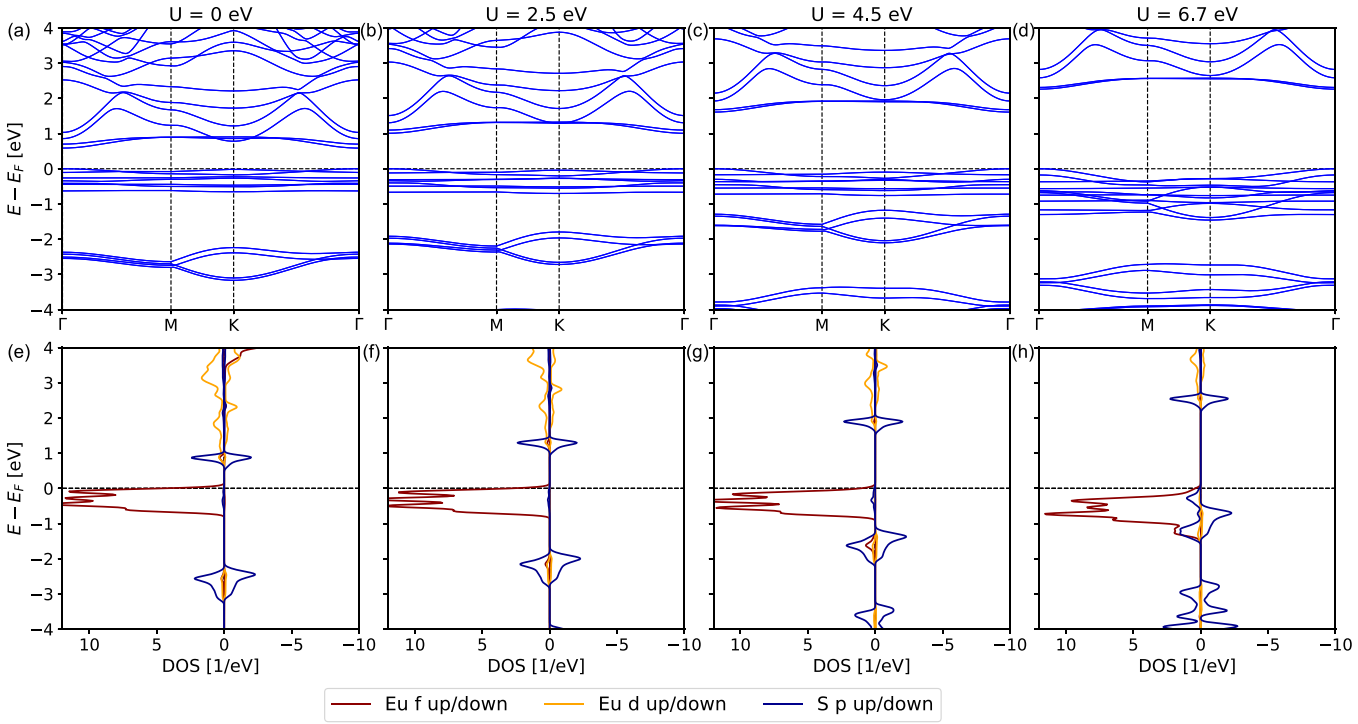

FIG. 2. Electronic structure of the H-phase EuS_2 monolayer as a function of Coulomb repulsion strength U. In (a)–(d) the band structures are shown for $U = 0$, 2.5, 4.5, and 6.7 eV, respectively. In (e)–(h) the corresponding evolution of the spin-resolved density of states is shown. In (e)–(h) the left and right parts of the plots correspond to the majority and minority spins, respectively, while the densities of states of Eu f, Eu d, and S p states are shown with dark red, orange, and blue thin lines, respectively. While the dominance of the majority Eu f states at the Fermi level is evident, increasing U drives the hybridization of Eu f states with S p states. This has a drastic influence on the transport properties of the system, as discussed in the text.

and 2(f)], 4.5 eV [Figs. 2(c) and 2(g)], and 6.7 eV [Figs. 2(d) and 2(h)]. The quantitative features of the electronic structure of EuS_2 are similar irrespective of U: The highest occupied states are formed by the Eu $4f$ majority electrons. The position of the minority f states varies from about $+4$ eV for $U = 0$ eV to about $+10$ eV for $U = 6.7$ eV, and we do not discuss these states further. The valence band maximum is positioned at the Γ point. We find p states of the chalcogen S atoms well separated and lying above and below the majority f states. Together with Eu f and d states the p states of S form bonding and antibonding states that have an energy separation of about 3.5 eV irrespective of the spin channel. The lowest conduction band is relatively flat, and it is formed by states with primarily S p character. The conduction band minimum is also positioned at the Γ point, and the EuS_2 monolayer exhibits a direct band gap of f-p transition. The higher conduction bands following the S p band are formed by highly dispersing Eu $6s$ and $5d$ states. The localized occupied $4f$ states act as a repulsive scattering potential to the S p electrons which moves bonding and antibonding S p states in the majority and minority spin channels to lower and higher energies, respectively. This introduces a small exchange splitting, visible in Figs. 2(a)–2(d), and a magnetic moment of $-0.28\mu_B$ on S atoms. The values of the orbital moments of Eu and S atoms are practically negligible.

Focusing on the $4f$ states, in the ground state, at $U = 0$ eV, the majority f states are separated from the conduction S p states by about 1 eV [direct band gap of 0.59 eV at Γ; see Figs. 2(a) and 2(e)]. Increasing U leads to an increase of the f-p gap without a change in dispersion, and the $4f$ states move down in energy closer to the occupied S p valence states (or, alternatively, since the Fermi energy is fixed by the band edge of the majority $4f$ states, the S p states move up in energy with respect to the f states). At $U = 6.7$ eV this results in a p-f energy separation of about 3 eV at the Fermi energy [direct band gap of 2.27 eV at Γ; Figs. 2(d) and 2(h)]. This puts EuS_2 among the large band gap TMD semiconductors [56,57]. On the other hand, increasing U drives the lower p states into the region of majority f states. In turn, this drives a strong hybridization between the p, d, and f states, which results in the orbital complexity and strong modifications that U brings to transport properties of the doped system which we discuss below. We conclude at this point that the EuS_2 monolayer is a ferromagnetic semiconductor with a direct band gap, whose value depends on the choice of U. The studied system can be turned into a half metal upon replacing Eu by, e.g., Gd, forming an $Eu_{1-x}Gd_xS_2$ layer.

B. Anomalous Hall effect in EuS_2

Next, we proceed to investigate the AHE in the system. Here, we focus on the intrinsic Berry curvature contribution to the AHC tensor [58]. To compute the Berry curvature from MLWF we first construct a tight-binding MLWF Hamiltonian

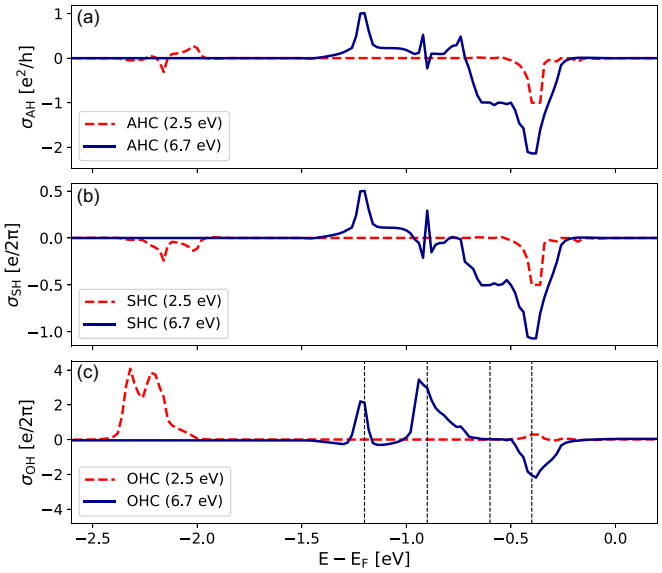

FIG. 3. Transport properties of monolayer EuS_2 as a function of band filling. (a) Anomalous Hall conductivity (AHC) σ_{AH}, (b) spin Hall conductivity (SHC) σ_{SH}, and (c) orbital Hall conductivity (OHC) σ_{OH}, computed as a function of band filling in EuS_2 for $U = 2.5$ eV (red dashed line) and 6.7 eV (blue solid line). Vertical dashed lines in (c) are guides to the eye marking the position of energy at -1.2, -0.9, -0.6, and -0.4 eV. The influence of S-Eu hybridization at $U = 6.7$ eV is clearly visible in the plot: while in the case of weak hybridization at $U = 2.5$ eV the AHE and SHE in the system are suppressed, the combined effect of interacting S p and Eu f states on the overall magnitude and complex behavior of the AHE, SHE, and OHE at $U = 6.7$ eV just below the Fermi energy is drastic.

and use the Wannier interpolation technique to efficiently evaluate the xy component of the AHC σ_{AH} as a Brillouin zone integral on a 300×300 mesh of k points according to the expression:

$$\sigma_{AH} = -\frac{e^2}{\hbar} \sum_n \int_{BZ} \frac{d^2\boldsymbol{k}}{(2\pi)^2} f_{n\boldsymbol{k}}\, \Omega_{n\boldsymbol{k}}, \tag{1}$$

with $f_{n\boldsymbol{k}}$ being the Fermi-Dirac distribution function and the Berry curvature $\Omega_{n\mathbf{k}}$ of a state n at point $\boldsymbol{k}$ being given by

$$\Omega_{n\boldsymbol{k}} = 2\hbar^2 \sum_{n \neq m} \mathrm{Im}\left[\frac{\langle u_{n\boldsymbol{k}}|v_x|u_{m\boldsymbol{k}}\rangle\langle u_{m\boldsymbol{k}}|v_y|u_{n\boldsymbol{k}}\rangle}{(E_{n\boldsymbol{k}} - E_{m\boldsymbol{k}} + i\eta)^2}\right], \tag{2}$$

where $E_{n\boldsymbol{k}}$ is the energy of a Bloch state with the lattice-periodic part of Bloch wave function given by $u_{n\boldsymbol{k}}$ and v_i is the ith Cartesian component of the velocity operator. To improve the convergence, we set $\eta = 25$ meV.

The results of our calculations of the AHC are summarized in Fig. 3(a) for the cases of $U = 2.5$ and 6.7 eV, of which we first discuss the former. The energy dependence of the AHC for $U = 2.5$ eV is shown with a dashed line in Fig. 3(a), where we observe that the AHC is nonzero only in narrow windows between -0.6 and $+0$ eV and -3 and -2 eV. They correspond to the upper region of majority f states and the region of occupied S p states, respectively. The out-of-plane spin and orbital polarization of these states is shown in Figs. 4(a) and 4(b). We observe that the low-lying p states are slightly exchange split (by 50–100 meV) and perfectly spin polarized, and they display very strong orbital polarization, especially at the top and bottom of the group. This is consistent with the process of $p_x \pm p_y$ orbital polarization, confirmed by the DOS analysis (not shown), giving rise to nontrivial Chern numbers and a nonvanishing AHC in the region of these states [59]. By inspecting the region of f states in Figs. 4(a) and 4(b) more closely, we observe the formation of relatively large gaps among the groups of f states, separated by the combined effect of crystal field and spin-orbit interaction. The topological nature of these gaps is predominantly trivial; that is, the quantized value of the AHC within these gaps is topologically trivial, except for the case of the gap at about -0.4 eV, where the AHC is quantized to a value of $-1\,\frac{e^2}{h}$ (i.e., having a Chern number of -1). From the analysis of the orbital character of contributing states it is clear that this is the region where the overall change in the sign of orbital polarization of the states around the gap takes place. This change in the orbital polarization across the gap mediated by the spin-conserving part of spin-orbit interaction can be closely associated with the nontrivial AHC in this region [59].

At this point we would like to comment on the logic behind the energy-resolved orbital polarization of the system for $U = 2.5$ eV. For this correlation strength, the Eu f states are separated from the p states of S atoms. The $4f$ electrons are localized and experience a nonspherical potential exhibiting the point group symmetry of the Eu atom embedded in the EuS_2 monolayer. Therefore, the development of the orbital moments is a result of a competition between Coulomb interaction, summarized under Hund's second rule, and the crystal field. We notice that our results still resemble Hund's second and third rules [Figs. 4(a) and 4(b)]. In the lower half of the $4f$ majority states, the orbital moment is opposite to the spin moment, while for the upper half of the $4f$ states the orbital moment is parallel to the spin moment, which results in a negligible orbital moment when summed over all majority $4f$ states. For S $4p$ states the situation is very different since the p states are subject to a large band dispersion where crystal field effects dominate. For states along Γ-M the dispersion of the S p states is rather small, and Hund's third rule is obeyed since the orbital moments of the lower (upper) half of the bands is antiparallel (parallel) to the spin moments, but the strong crystal field associated with the band dispersion along the high-symmetry lines M-K-Γ makes Hund's third rule inapplicable. This violation becomes even more prominent for larger values of the correlation strength.

The effect of direct interaction between the p states of S and f states of Eu, which takes place when we increase the correlation strength to $U = 6.7$ eV, has a profound effect on the AHE. From the analysis of the DOS and spin polarization of the states shown in Fig. 4(c) we observe that minority p states are easily identifiable as they do not at all hybridize with the f states of opposite spin. The hybridization of the majority p and f states is, on the other hand, drastic, which is evidenced by strong changes in the position and dispersion of the bands, as well as increased spread of Eu and S states over the region of almost 1.5 eV in energy for this spin channel. The resulting orbital complexity of hybridized states, visible in Fig. 4(c), has an amplifying effect on the overall magnitude of the

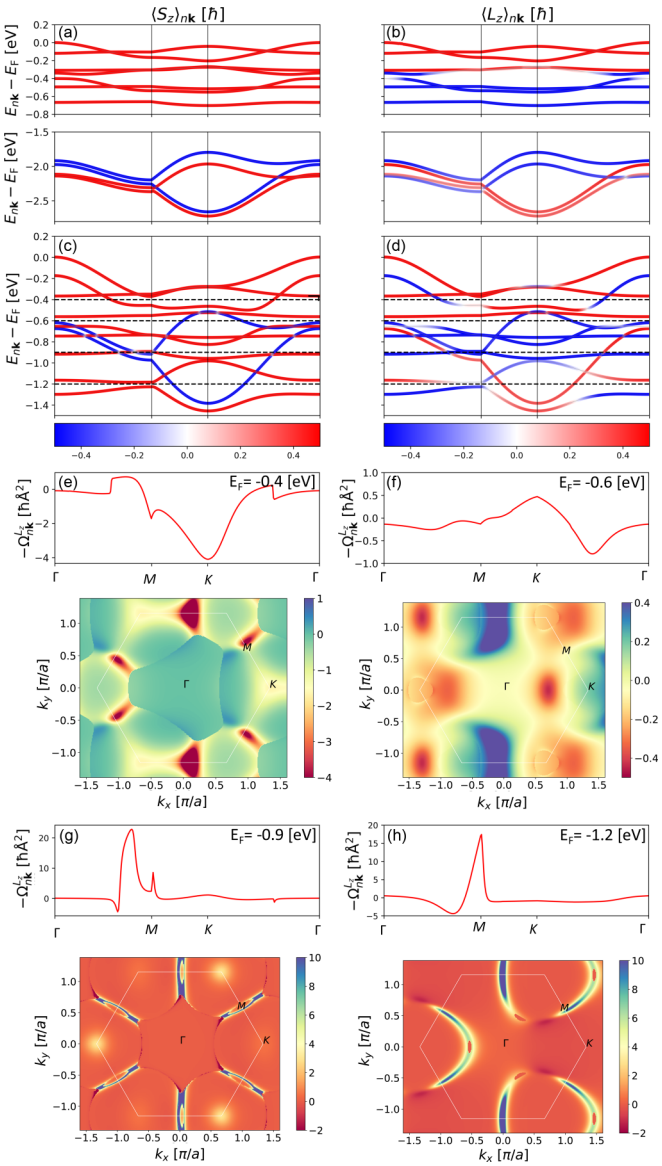

FIG. 4. Evolution of (a) and (c) the out-of-plane spin $\langle S_z\rangle_{n\mathbf{k}}$ and (b) and (d) orbital polarization $\langle L_z\rangle_{n\mathbf{k}}$ of occupied states in EuS_2. (a) The occupied spin-up f states of Eu above -0.8 eV (top) and S p states in the region between -3 and -1.5 eV (bottom) for the case of $U = 2.5$ eV. Note that both groups of displayed states are isolated in energy from other states. (c) The hybridized group of occupied f and p states for the case of $U = 6.7$ eV which reside above -1.5 eV. (b) and (d) are analogous to (a) and (c). The value scales are indicated by the color bars at the bottom in units of $\hbar$. Horizontal dashed lines in (c) and (d) are guides to the eye marking the position of energy at -1.2, -0.9, -0.6, and -0.4 eV. (e), (f), (g) and (h) Distribution of the orbital Berry curvature along high-symmetry lines for the indicated position of the Fermi energy, shown together with the distribution of the corresponding orbital Berry curvature in the Brillouin zone.

AHC. In particular, close to quantized values of the AHC are achieved for the lower bands around -1.2 eV ($\sigma_{\mathrm{AH}} \approx +1\,\frac{e^2}{\hbar}$, related to a global gap present there, crossed by minority S states), a wide plateau around -0.6 eV (with $\sigma_{\mathrm{AH}} \approx -1\,\frac{e^2}{\hbar}$, related to the nontrivial gap between three upper and five lower majority bands, separated by an "inactive" band at -0.55 eV), and a peak at -0.4 eV (with $\sigma_{\mathrm{AH}} \approx -2\,\frac{e^2}{h}$).

C. Spin Hall effect in EuS_2

We now move on to the study of the SHE and OHE in the system. While the SHE has been explicitly studied in group-VI dichalcogenides [11,12], very recently, Canonico and coworkers investigated the orbital Hall effect in the nonmagnetic H-phase 2D TMDs MoS_2 and WS_2 [14,16], addressing especially the question of quantization of the OHC within the electronic energy gaps and the corresponding emergence of the quantum orbital Hall insulating phase. The study of the OHE is a subject of general interest since the magnitude of the OHC can often be dominant over that of the SHC, which suggests systems with a large OHE as a potential platform for novel concepts in orbitronics [35,60].

Motivated by these considerations, we proceed to explore the possibility that EuS_2 can host SHE and OHE. Following the established methodology [22,61], we calculate the SHC and OHC, which mediates the generation of a transverse in-plane current of out-of-plane (spin or orbital) angular momentum in response to an applied electric field, according to the Kubo expression:

$$\sigma_{\mathrm{OH/SH}} = \frac{e}{\hbar}\sum_n \int \frac{d^2\boldsymbol{k}}{(2\pi)^2} f_{n\boldsymbol{k}}\,\Omega^{J_z}_{n\boldsymbol{k}}, \tag{3}$$

where the so-called spin (orbital) Berry curvature reads

$$\Omega^{J_z}_{n\boldsymbol{k}} = 2\hbar^2 \sum_{m\neq n} \mathrm{Im}\left[\frac{\langle u_{n\boldsymbol{k}}|j_y^{J_z}|u_{m\boldsymbol{k}}\rangle\langle u_{m\boldsymbol{k}}|v_x|u_{m\boldsymbol{k}}\rangle}{(E_{n\boldsymbol{k}} - E_{m\boldsymbol{k}} + i\eta)^2}\right], \tag{4}$$

with $j_y^{J_z}$ being the spin ($J_z = S_z$, the z component of the spin operator) or orbital ($J_z = L_z$, the z component of the local angular momentum operator) current operator defined as $j_y^{J_z} = (v_y J_z + J_z v_y)/2$.

We first look at the SHE, presenting the results of the calculations in Fig. 3(b). For the case of $U = 2.5$ eV we find that for the f states the SHC precisely follows the AHC as the band filling is varied. This is consistent with the picture of the spin angular momentum carried by the anomalous Hall current of fully spin polarized f bands in that energy region. The behavior of the SHC of S p states at lower energies is more complicated; however, the consistently negative sign of the SHC can be understood from the sign reversal both in net spin polarization and in the AHC at the top and bottom of the S states. Remarkably, an almost perfect one-to-one correspondence between the energy dependences of the SHC and AHC still persists for a more complex case of $U = 6.7$ eV. This can be, again, understood by taking into account the pure spin character of f states. The presence in that energy region of minority S states [see Figs. 4(c) and 4(d)] is the reason for a discrepancy in the shape of the SHC and AHC between -1.0 and -0.6 eV, which can be explained by taking into account the small negative spin Hall signal that the minority S states bring with them into that energy region.

D. Orbital Hall effect in EuS_2

Finally, we turn to the analysis of the OHE in the system. We present the results of our calculations of the OHC in Fig. 3(c). We first observe that in the "unhybridized" case of $U = 2.5$ eV, the OHC of f states is minimal, reaching in magnitude the SHC in the region around -0.4 eV, where the AHE and SHE are present as well. Most remarkable is the gigantic OHE carried by the p states of S atoms, positioned between -3 and -2 eV [Fig. 4(b)]. The OHC in this region is almost one order of magnitude larger than the SHC or OHC of the f states for this value of U. By inspecting the correlation between the electronic structure, orbital polarization, and orbital Hall conductivity, we can identify a region of energy between -2.4 and -2.1 eV as the dominant source of the OHE due to contributions coming from crossings among bands of different orbital characters, clearly visible close to the M point and the Γ point in Fig. 4(b), as well as larger parts of the Brillouin zone where there is strong k-dependent exchange of orbital angular momentum among the oppositely polarized bands, which is a direct consequence of the k-dependent hybridization strength.

Upon increasing the value of U to 6.7 eV the complicated p-d-f hybridization taking place among S and Eu atoms exerts a striking influence on the properties of the OHE of the p-f group of states below the Fermi energy. This is reflected in a 3 to 4 times larger magnitude of the OHC compared to the SHC observed in the region of majority f states [Fig. 3(c)] and, in contrast to expectations from oversimplifying band-filling arguments applied in the past to nonmagnetic materials [19], a very nontrivial dependence of the OHC on the Fermi energy. At first, it is tempting to attribute the large computed OHC to S p states, which promote a strong OHE already for smaller values of U without any need for aid from the side of f orbitals. However, a closer analysis shows that this is not the case.

First, we take a look at the region of energy around -1.2 eV, where the lowest of the peaks in the OHC appears [this energy value is indicated with dashed lines in Figs. 3(c), 4(c), and 4(d)]. Here, the large peak in the OHC originates from an anticrossing among two strongly Eu-S hybridized bands [see also the corresponding DOS in Fig. 2(h)], positioned at that energy, where an exchange of the orbital polarization is particularly visible around the M point. A very similar situation is encountered next to and directly at the M point around $E_F = -0.9$ eV, where the crucial role of the orbital angular momentum exchange and large values of the OHC displayed by the majority p states become very apparent. The distribution of the orbital Berry curvature of occupied states up to the corresponding Fermi energy, shown in Figs. 4(g) and 4(h), confirms this picture. From the k-space distribution of the orbital Berry curvature we observe that large OHE at these energies originates from sharp circular features centered around K' points in the Brillouin zone.

Despite the sizable magnitude of the AHC and SHC in the region of energy between -0.7 and -0.5 eV [the value of -0.6 eV is marked with dashed lines in Figs. 3(c), 4(c) and 4(d)], the OHC is suppressed there, which is quite unexpected. The reason for this is the absence of the k-dependent exchange of the orbital polarization among pairs of bands, which appear in this energy window. Although there is a crossing of positively and negatively orbitally polarized bands around -0.55 eV in the vicinity of the K point, no hybridization or exchange of orbital angular momentum takes place there. The corresponding orbital Berry curvature for this Fermi energy, shown in Fig. 4(f), is overall more than one order of magnitude smaller than that for the previously considered cases. This solidifies the k-dependent orbital polarization exchange as a driving force behind the large OHE observed in the studied system at lower energies.

The scenario for the large OHC in the vicinity of -0.4 eV is different: Here, it is the orbital exchange around M and K, taking place among pairs of bands well separated in energy, i.e., the second and third bands when counting down from zero energy. While this gives rise to moderate negative values of the orbital Berry curvature over larger regions of the reciprocal space around K, smaller regions of reciprocal space around M and especially M' contribute prominently to the overall sizable OHC [Fig. 4(e)]. The negative sign of the OHC here, which cannot be achieved with either p or f states separately (for lower U), emphasizes once more the importance of the p-f hybridization for the orbital Hall physics in EuS_2 in particular and in rare-earth dichalcogenides in general.

IV. DISCUSSION

The main motivation behind our work was the exploration of possible benefits that the combination of chalcogenides with f elements in 2D geometry can bring. Here, we chose EuS_2 as a representative of this class of materials. One of the strongest points of this type of system, besides the very prominent magnetism that f electrons exhibit, is the strong spin-orbit interaction mediated by the f states. This is a very robust and unique feature which is very difficult to achieve with other types of TMDs, where magnetism is much more fragile and the influence of the structure on the nature of exchange-split bands is much stronger. Combined with the orbital complexity of f states, robust magnetism has the potential to give rise to topologically nontrivial anomalous and spin Hall effects. While the strong localization of f states naturally suppresses interatomic hybridization among atoms of f species, the expectation is that the hybridization with highly dispersive p states of chalcogenides will aid in promoting strong Hall effects that are unachievable either by a pure f system or by at best slightly magnetized p bands. Fostering strong hybridization between f and p atoms thus presents a material challenge. At the same time, while it is known that even nonmagnetic p systems can host large orbital transport properties, a material system which exhibits very large anomalous, spin, and orbital Hall effects at the same time is not yet known. In this context, rare-earth dichalcogenides thus present an exciting platform for the realization of pronounced transport phenomena of a diverse nature.

With our work we attempt to initiate focused research on the discovery and characterization of rare-earth dichalcogenides by showing that exciting properties listed above can be achieved in principle. In the course of our study of structural, electronic, magnetic, and transport properties of EuS_2 from first principles we expectedly found that EuS_2 exhibits pronounced magnetism. We also found that this f material

gives rise to very strong Hall responses and hosts topologically nontrivial bands, despite strong correlation among electrons in the f shell. We identified that the reason for this is a strong degree of p-d-f hybridization among the Eu and S atoms, enhanced by stronger correlation effects owing to the peculiar electronic structure of EuS_2. Effectively, the S-originated p states and Eu f states unite their efforts in enhancing each other's anomalous and spin Hall responses. As a result of complex orbital hybridization among the latter states, the composite p-f group of states also exhibits a very large orbital Hall effect, which is dominant over the SHE by about a factor of 3. We identify k-dependent orbital exchange among pairs of hybridized bands as the major source and physical mechanism of the large and nontrivial orbital Hall effect, which should be explored further as the possible governing force behind the large orbital Hall effect in magnetic materials in general.

Concerning the feasibility of experimental observation of the studied system, we have to remark that several compounds of Eu with chalcogenides are experimentally known in the bulk, at interfaces, and in thin films, e.g., based on EuS [62–66], $EuSe_2$ [67], and $EuTe_2$ [68]. We thus believe that thin two-dimensional layers of EuS_2 can be naturally produced using, for example, exfoliation or molecular beam epitaxy. On the other hand, the general conclusions of our work are valid for the entire class of two-dimensional rare-earth dichalcogenides, marking them as an exciting platform for spin and orbital physics and advancing our understanding of complex orbital transport manifestations of correlated magnetic two-dimensional materials.

ACKNOWLEDGMENTS

This work was supported by the Federal Ministry of Education and Research of Germany in the framework of the Palestinian-German Science Bridge (BMBF Grant No. 01DH16027). We also gratefully acknowledge financial support from the Deutsche Forschungsgemeinschaft (DFG, German Research Foundation), TRR 288 – 422213477 (Project No. B06), TRR 173/2 – 268565370 (Projects No. A11 and No. A01), and CRC 1238 – 277146847 (Project No. C01), and the Sino-German research project DISTOMAT (MO 1731/10-1). We also gratefully acknowledge the Jülich Supercomputing Centre and RWTH Aachen University for providing computational resources under projects jiff40 and jara0062.

[1] A. Splendiani, L. Sun, Y. Zhang, T. Li, J. Kim, C.-Y. Chim, G. Galli, and F. Wang, Emerging photoluminescence in monolayer MoS_2, Nano Lett. **10**, 1271 (2010).

[2] H. R. Gutiérrez, N. Perea-López, A. L. Elías, A. Berkdemir, B. Wang, R. Lv, F. López-Urías, V. H. Crespi, H. Terrones, and M. Terrones, Extraordinary room-temperature photoluminescence in triangular WS_2 monolayers, Nano Lett. **13**, 3447 (2013).

[3] P. Miró, M. Ghorbani-Asl, and T. Heine, Two dimensional materials beyond MoS_2: Noble-transition-metal dichalcogenides, Angew. Chem. **53**, 3015 (2014).

[4] C.-H. Lee, E. C. Silva, L. Calderin, M. A. T. Nguyen, M. J. Hollander, B. Bersch, T. E. Mallouk, and J. A. Robinson, Tungsten ditelluride: A layered semimetal, Sci. Rep. **5**, 10013 (2015).

[5] S. Zhao, T. Hotta, T. Koretsune, K. Watanabe, T. Taniguchi, K. Sugawara, T. Takahashi, H. Shinohara, and R. Kitaura, Two-dimensional metallic NbS_2: Growth, optical identification and transport properties, 2D Mater. **3**, 025027 (2016).

[6] I. Guillamón, H. Suderow, J. G. Rodrigo, S. Vieira, P. Rodière, L. Cario, E. Navarro-Moratalla, C. Martí-Gastaldo, and E. Coronado, Chiral charge order in the superconductor 2H-TaS_2, New J. Phys. **13**, 103020 (2011).

[7] Z. Y. Zhu, Y. C. Cheng, and U. Schwingenschlögl, Giant spin-orbit-induced spin splitting in two-dimensional transition-metal dichalcogenide semiconductors, Phys. Rev. B **84**, 153402 (2011).

[8] H.-R. Fuh, B. Yan, S. Wu, C. Felser, and C. Chang, Metal-insulator transition and the anomalous Hall effect in the layered magnetic materials VS_2 and VSe_2, New J. Phys. **18**, 113038 (2016).

[9] K. F. Mak, K. L. McGill, J. Park, and P. L. McEuen, The valley Hall effect in MoS_2 transistors, Science **344**, 1489 (2014).

[10] X. Zhou, R. Zhang, Z. Zhang, W. Feng, Y. Mokrousov, and Y. Yao, Sign-reversible valley-dependent Berry phase effects in 2D valley-half-semiconductors, npj Comput. Mater. **7**, 160 (2021).

[11] W. Feng, Y. Yao, W. Zhu, J. Zhou, W. Yao, and D. Xiao, Intrinsic spin Hall effect in monolayers of group-VI dichalcogenides: A first-principles study, Phys. Rev. B **86**, 165108 (2012).

[12] D. Xiao, G.-B. Liu, W. Feng, X. Xu, and W. Yao, Coupled Spin and Valley Physics in Monolayers of MoS_2 and Other Group-VI Dichalcogenides, Phys. Rev. Lett. **108**, 196802 (2012).

[13] T. P. Cysne, M. Costa, L. M. Canonico, M. B. Nardelli, R. B. Muniz, and T. G. Rappoport, Disentangling Orbital and Valley Hall Effects in Bilayers of Transition Metal Dichalcogenides, Phys. Rev. Lett. **126**, 056601 (2021).

[14] L. M. Canonico, T. P. Cysne, T. G. Rappoport, and R. B. Muniz, Two-dimensional orbital Hall insulators, Phys. Rev. B **101**, 075429 (2020).

[15] S. Bhowal and S. Satpathy, Intrinsic orbital and spin Hall effects in monolayer transition metal dichalcogenides, Phys. Rev. B **102**, 035409 (2020).

[16] L. M. Canonico, T. P. Cysne, A. Molina-Sanchez, R. B. Muniz, and T. G. Rappoport, Orbital Hall insulating phase in transition metal dichalcogenide monolayers, Phys. Rev. B **101**, 161409(R) (2020).

[17] Y. Liu, Y. Gao, S. Zhang, J. He, J. Yu, and Z. Liu, Valleytronics in transition metal dichalcogenides materials, Nano Res. **12**, 2695 (2019).

[18] B. A. Bernevig, T. L. Hughes, and S.-C. Zhang, Orbitronics: The Intrinsic Orbital Current in p-Doped Silicon, Phys. Rev. Lett. **95**, 066601 (2005).

[19] T. Tanaka, H. Kontani, M. Naito, T. Naito, D. S. Hirashima, K. Yamada, and J. Inoue, Intrinsic spin Hall effect and orbital Hall effect in 4d and 5d transition metals, Phys. Rev. B **77**, 165117 (2008).

[20] D. Jo, D. Go, and H.-W. Lee, Gigantic intrinsic orbital Hall effects in weakly spin-orbit coupled metals, Phys. Rev. B **98**, 214405 (2018).

[21] H. Kontani, T. Tanaka, D. S. Hirashima, K. Yamada, and J. Inoue, Giant Orbital Hall Effect in Transition Metals: Origin of Large Spin and Anomalous Hall Effects, Phys. Rev. Lett. **102**, 016601 (2009).

[22] D. Go, D. Jo, C. Kim, and H.-W. Lee, Intrinsic Spin and Orbital Hall Effects from Orbital Texture, Phys. Rev. Lett. **121**, 086602 (2018).

[23] T. P. Cysne, S. Bhowal, G. Vignale, and T. G. Rappoport, Orbital Hall effect in bilayer transition metal dichalcogenides: From the intra-atomic approximation to the Bloch states orbital magnetic moment approach, Phys. Rev. B **105**, 195421 (2022).

[24] W.-Y. Shan, H.-Z. Lu, and D. Xiao, Spin Hall effect in spin-valley coupled monolayers of transition metal dichalcogenides, Phys. Rev. B **88**, 125301 (2013).

[25] S. Bhowal and S. Satpathy, Electronic structure and anomalous Hall effect in the ferromagnetic $3d-5d$ superlattice $SrMnO_3/SrIrO_3$, Phys. Rev. B **99**, 245145 (2019).

[26] S. Bhowal and S. Satpathy, Dirac nodal lines and large spin Hall effect in the $6H$-perovskite iridate $Ba_3TiIr_2O_9$, Phys. Rev. B **100**, 115101 (2019).

[27] J.-Y. You, C. Chen, Z. Zhang, X.-L. Sheng, S. A. Yang, and G. Su, Two-dimensional Weyl half-semimetal and tunable quantum anomalous Hall effect, Phys. Rev. B **100**, 064408 (2019).

[28] J. Sinova, S. O. Valenzuela, J. Wunderlich, C. H. Back, and T. Jungwirth, Spin Hall effects, Rev. Mod. Phys. **87**, 1213 (2015).

[29] S. Bhowal and S. Satpathy, Intrinsic orbital moment and prediction of a large orbital Hall effect in two-dimensional transition metal dichalcogenides, Phys. Rev. B **101**, 121112(R) (2020).

[30] I. V. Tokatly, Orbital momentum Hall effect in p-doped graphane, Phys. Rev. B **82**, 161404(R) (2010).

[31] S. Bhowal and G. Vignale, Orbital Hall effect as an alternative to valley Hall effect in gapped graphene, Phys. Rev. B **103**, 195309 (2021).

[32] D. Go and H.-W. Lee, Orbital torque: Torque generation by orbital current injection, Phys. Rev. Research **2**, 013177 (2020).

[33] S. Lee, M.-G. Kang, D. Go, D. Kim, J.-H. Kang, T. Lee, G.-H. Lee, J. Kang, N. J. Lee, Y. Mokrousov, S. Kim, K.-J. Kim, K.-J. Lee, and B.-G. Park, Efficient conversion of orbital hall current to spin current for spin-orbit torque switching, Commun. Phys. **4**, 1 (2021).

[34] D. Go, F. Freimuth, J.-P. Hanke, F. Xue, O. Gomonay, K.-J. Lee, S. Blügel, P. M. Haney, H.-W. Lee, and Y. Mokrousov, Theory of current-induced angular momentum transfer dynamics in spin-orbit coupled systems, Phys. Rev. Research **2**, 033401 (2020).

[35] D. Go, D. Jo, T. Gao, K. Ando, S. Blügel, H.-W. Lee, and Y. Mokrousov, Orbital Rashba effect in a surface-oxidized Cu film, Phys. Rev. B **103**, L121113 (2021).

[36] M. Gibertini, M. Koperski, A. Morpurgo, and K. Novoselov, Magnetic 2D materials and heterostructures, Nat. Nanotechnol. **14**, 408 (2019).

[37] B. Zhai, J. Du, X. Li, C. Xia, and Z. Wei, Two-dimensional ferromagnetic materials and related van der Waals heterostructures: A first-principle study, J. Semicond. **40**, 081509 (2019).

[38] Q. Shao, P. Li, L. Liu, H. Yang, S. Fukami, A. Razavi, H. Wu, K. Wang, F. Freimuth, Y. Mokrousov, M. D. Stiles, S. Emori, A. Hoffmann, J. Ãkerman, K. Roy, J.-P. Wang, S.-H. Yang, K. Garello, and W. Zhang, Roadmap of spin-orbit torques, IEEE Trans. Magn. **57**, 1 (2021).

[39] B. Huang, G. Clark, E. Navarro-Moratalla, D. R. Klein, R. Cheng, K. L. Seyler, D. Zhong, E. Schmidgall, M. A. McGuire, D. H. Cobden, W. Yao, D. Xiao, P. Jarillo-Herrero, and X. Xu, Layer-dependent ferromagnetism in a van der Waals crystal down to the monolayer limit, Nature (London) **546**, 270 (2017).

[40] Y. Deng, Y. Yu, Y. Song, J. Zhang, N. Z. Wang, Z. Sun, Y. Yi, Y. Z. Wu, S. Wu, J. Zhu, J. Wang, X. H. Chen, and Y. Zhang, Gate-tunable room-temperature ferromagnetism in two-dimensional Fe_3GeTe_2, Nature (London) **563**, 94 (2018).

[41] C. Gong, L. Li, Z. Li, H. Ji, A. Stern, Y. Xia, T. Cao, W. Bao, C. Wang, Y. Wang, Z. Q. Qiu, R. J. Cava, S. G. Louie, J. Xia, and X. Zhang, Discovery of intrinsic ferromagnetism in two-dimensional van der Waals crystals, Nature (London) **546**, 265 (2017).

[42] F. Zhu, L. Zhang, X. Wang, F. J. dos Santos, J. Song, T. Mueller, K. Schmalzl, W. F. Schmidt, A. Ivanov, J. T. Park, J. Xu, J. Ma, S. Lounis, S. Blügel, Y. Mokrousov, Y. Su, and T. Brückel, Topological magnon insulators in two-dimensional van der Waals ferromagnets $CrSiTe_3$ and $CrGeTe_3$: Toward intrinsic gap-tunability, Sci. Adv. **7**, eabi7532 (2021).

[43] H. Pan, Magnetic and electronic evolutions of hydrogenated VTe_2 monolayer under tension, Sci. Rep. **4**, 7524 (2014).

[44] Y. Ma, Y. Dai, M. Guo, C. Niu, Y. Zhu, and B. Huang, Evidence of the existence of magnetism in pristine VX_2 monolayers (X = S, Se) and their strain-induced tunable magnetic properties, ACS Nano **6**, 1695 (2012).

[45] W. Chen, J. Zhang, Y. Nie, Q. Xia, and G. Guo, Electronic structure and magnetism of MTe_2 (M = Ti, V, Cr, Mn, Fe, Co and Ni), J. Magn. Magn. Mater. **508**, 166878 (2020).

[46] C. Wang, X. Zhou, Y. Pan, J. Qiao, X. Kong, C.-C. Kaun, and W. Ji, Layer and doping tunable ferromagnetic order in two-dimensional CrS_2 layers, Phys. Rev. B **97**, 245409 (2018).

[47] H. Y. Lv, W. J. Lu, D. F. Shao, Y. Liu, and Y. P. Sun, Strain-controlled switch between ferromagnetism and antiferromagnetism in $1T$-CrX_2 (X = Se, Te) monolayers, Phys. Rev. B **92**, 214419 (2015).

[48] C. Ataca, H. Şahin, and S. Ciraci, Stable, single-layer MX_2 transition-metal oxides and dichalcogenides in a honeycomb-like structure, J. Phys. Chem. C **116**, 8983 (2012).

[49] M. Kan, S. Adhikari, and Q. Sun, Ferromagnetism in MnX_2 (X = S, Se) monolayers, Phys. Chem. Chem. Phys. **16**, 4990 (2014).

[50] E. Wimmer, H. Krakauer, M. Weinert, and A. J. Freeman, Full-potential self-consistent linearized-augmented-plane-wave method for calculating the electronic structure of molecules and surfaces: O_2 molecule, Phys. Rev. B **24**, 864 (1981).

[51] For the FLEUR program description, see https://www.flapw.de.

[52] J. P. Perdew, K. Burke, and M. Ernzerhof, Generalized Gradient Approximation Made Simple, Phys. Rev. Lett. **77**, 3865 (1996).

[53] A. B. Shick, A. I. Liechtenstein, and W. E. Pickett, Implementation of the LDA+U method using the full-potential linearized augmented plane-wave basis, Phys. Rev. B **60**, 10763 (1999).

[54] G. Pizzi, V. Vitale, R. Arita, S. Blügel, F. Freimuth, G. Géranton, M. Gibertini, D. Gresch, C. Johnson, T. Koretsune *et al.*, Wannier90 as a community code: New features and applications, J. Phys.: Condens. Matter **32**, 165902 (2020).

[55] F. Freimuth, Y. Mokrousov, D. Wortmann, S. Heinze, and S. Blügel, Maximally localized Wannier functions within the FLAPW formalism, Phys. Rev. B **78**, 035120 (2008).

[56] H. Guo, N. Lu, L. Wang, X. Wu, and X. C. Zeng, Tuning electronic and magnetic properties of early transition-metal dichalcogenides via tensile strain, J. Phys. Chem. C **118**, 7242 (2014).

[57] Y. Jiao, L. Zhou, F. Ma, G. Gao, L. Kou, J. Bell, S. Sanvito, and A. Du, Predicting single-layer technetium dichalcogenides TcX_2 (X = S, Se) with promising applications in photovoltaics and photocatalysis, ACS Appl. Mater. Interfaces **8**, 5385 (2016).

[58] N. Nagaosa, J. Sinova, S. Onoda, A. H. MacDonald, and N. P. Ong, Anomalous Hall effect, Rev. Mod. Phys. **82**, 1539 (2010).

[59] H. Zhang, F. Freimuth, G. Bihlmayer, M. Ležaić, S. Blügel, and Y. Mokrousov, Engineering quantum anomalous Hall phases with orbital and spin degrees of freedom, Phys. Rev. B **87**, 205132 (2013).

[60] H. Kontani, T. Tanaka, D. S. Hirashima, K. Yamada, and J. Inoue, Giant Intrinsic Spin and Orbital Hall Effects in Sr_2MO_4 (M = Ru, Rh, Mo), Phys. Rev. Lett. **100**, 096601 (2008).

[61] D. Go, D. Jo, H.-W. Lee, M. Kläui, and Y. Mokrousov, Orbitronics: Orbital currents in solids, Europhys. Lett. **135**, 37001 (2021).

[62] S. D. Pappas, P. Poulopoulos, B. Lewitz, A. Straub, A. Goschew, V. Kapaklis, F. Wilhelm, A. Rogalev, and P. Fumagalli, Direct evidence for significant spin-polarization of EuS in Co/EuS multilayers at room temperature, Sci. Rep. **3**, 1333 (2013).

[63] P. Poulopoulos, A. Goschew, V. Kapaklis, M. Wolff, A. Delimitis, F. Wilhelm, A. Rogalev, S. D. Pappas, A. Straub, and P. Fumagalli, Induced spin-polarization of EuS at room temperature in Ni/EuS multilayers, Appl. Phys. Lett. **104**, 112411 (2014).

[64] S. M. J. Beer, A. Muriqi, P. Lindner, M. Winter, D. Rogalla, M. Nolan, A. Ney, J. Debus, and A. Devi, Ferromagnetic europium sulfide thin films: Influence of precursors on magneto-optical properties, Chem. Mater. **34**, 152 (2022).

[65] C. J. P. Smits, A. T. Filip, J. T. Kohlhepp, H. J. M. Swagten, B. Koopmans, and W. J. M. de Jonge, Magnetic and structural properties of EuS for magnetic tunnel junction barriers, J. Appl. Phys. **95**, 7405 (2004).

[66] A. T. Filip, P. LeClair, C. J. P. Smits, J. T. Kohlhepp, H. J. M. Swagten, B. Koopmans, and W. J. M. de Jonge, Spin-injection device based on EuS magnetic tunnel barriers, Appl. Phys. Lett. **81**, 1815 (2002).

[67] J. A. Cowen, P. Michlin, J. Kraus, S. D. Mahanti, J. A. Aitken, and M. G. Kanatzidis, $EuSe_2$: A novel antiferromagnetic rare-earth polychalcogenide, J. Appl. Phys. **85**, 5381 (1999).

[68] J. Yin, C. Wu, L. Li, J. Yu, H. Sun, B. Shen, B. A. Frandsen, D.-X. Yao, and M. Wang, Large negative magnetoresistance in the antiferromagnetic rare-earth dichalcogenide $EuTe_2$, Phys. Rev. Materials **4**, 013405 (2020).